Designing Supertough and Ultrastretchable Liquid Metal-Embedded Natural Rubber Composites for Soft-Matter Engineering

Banerjee Shib Shankar, Mandal Subhradeep, Arief Injamamul, Layek Rama Kanta, Ghosh Anik Kumar, Yang Ke, Kumar Jayant, Formanek Petr, Fery Andreas, Heinrich Gert, Das Amit

DOI: 10.1021/acsami.1c00374

Designing super-tough and ultra-stretchable liquid metal embedded natural rubber composites for soft-matter engineering

Shib Shankar Banerjee[1,#], Subhradeep Mandal[1], Injamamul Arief[1], Ramakanta Layek[2], Anik Kumar Ghosh[1], Ke Yang[3], Jayant Kumar[3], Petr Formanek[1], Andreas Fery[1], Gert Heinrich[1,4], Amit Das[1,5]*

[1]Leibniz-Institut für Polymerforschung Dresden e. V, Hohe Straße 6, Dresden, 01069, Germany
[2]LUT University, Lahti, Mukkulankatu 19, FI-15210, Finland
[3]University of Massachusetts Lowell, Center for Advanced Materials, Department of Physics, MA 01854, USA
[4]Technische Universität Dresden, Institut für Textilmaschinen und Textile Hochleistungswerkstofftechnik, Hohe Straße 6, 01069 Dresden, Germany
[5]Tampere University, Engineering and Natural Sciences, FI-33101, Finland

Abstract:

Functional elastomers with incredible toughness and stretchability are indispensable for applications in soft robotics and wearable electronics. Furthermore, coupled with excellent electrical and thermal properties, these materials are at the forefront of recent efforts towards widespread use in cutting-edge electronics and devices. Herein, we introduce a highly deformable eutectic-GaIn liquid metal alloy-embedded natural rubber (NR) architecture employing, for the first time, industrially viable solid-state mixing and vulcanization. Standard methods of rubber processing and vulcanization allow us to fragment and disperse liquid metals into submicron-sized droplets in cross-linked NR without compromising the elastic properties of the base matrix. In addition to substantial boosts in mechanical (strain at failure of up to ~650 %) and elastic (negligible hysteresis loss) performances, the tearing energy of the composite was enhanced up to 6 times, and a four-fold reduction in crack growth rate was achieved over a control vulcanizate. Moreover, we demonstrate improved thermal conductivity and dielectric properties for the resulting composites. Therefore, this work provides a facile and scalable pathway to develop liquid metal-embedded soft elastomeric composites that could be instrumental towards potential applications in soft-matter engineering.

Keywords: soft rubber composites; liquid metal fillers; fracture toughness; tearing energy

***Corresponding author email: das@ipfdd.de**
#Present address**:** Department of Materials Science and Engineering, Indian Institute of Technology Delhi, Hauz Khas, New Delhi 110016, India.

1. INTRODUCTION

The ubiquitous presence of soft smart composites in various domains nowadays are primarily attributed to their uniquely customizable mechanical, chemical, thermal, and electrical properties, higher strength-to-weight ratio, and compatibility to biological tissues. Traditional electronics employing rigid materials pose limited functionalities that include lack of conformability, resistance to bending/stretching, and impact loading. On the other hand, excellent multifunctionality, stretchability, electrical and thermal conductivities of these soft yet robust elastomeric composites appear suitable in several high-end applications; namely bio-mimetic human tissues and artificial skin,[1] surgical assistant robots,[2-3] energy storage,[4] energy harvesting,[5] bio-hybrid engineering,[6] 1D/2D materials for flexible electronics,[7-8] sensors,[9-10] actuators,[1, 11] logic devices and electroluminescent.[12] To design and develop state-of-the-art devices for the said applications, incorporation of functionalized rigid fillers such as silver powders,[13] titanium dioxide,[14] lead-magnesium powders,[15] conducting carbon black,[16] carbon nanotubes,[17] etc. into the soft matrix is a necessary prerequisite. However, adequate functionalization often demands a copious amount of fillers to be blended into the matrix systems. This inevitably leads to poor elasticity, low flexibility, and high hardness of the hybrid composites.[18]

Elastomers represent a unique class of soft material systems due to their low mechanical compliance, lower cohesive energy density, and glass transition temperature (making them flexible in ambient conditions). However, commercial elastomers pose additional challenges in terms of cumbersome functionalization, inferior dielectric responses originating from thermal and electrical insulating characteristics.[19] Moreover, industrial elastomers seldom exhibit softness like biological tissue or skin.[19-20] To incorporate superior thermal/electrical conductivities into soft elastomeric systems, recent trends illustrate methods of blending functional fluids into elastomers. One such trend demonstrated attempts to fabricate a soft elastomeric system by incorporating liquid metals into liquid or gel rubbers like silicone and polyurethane with matching phases, resulting in composites with improved properties. Liquid metals (LM), while possessing high metallic electrical and thermal conductivities, can be used as a secondary phase to create polymer composites with the desired properties along with ultra-high elasticity. A broad category of liquid metals including Cs (melting point, MP ~28°C), Fr (MP ~27°C), Hg (MP ~-39°C), Rb (MP ~38°C), and Ga (MP ~29°C) has already been employed in various applications like microfluidic pumps,[21]

cooling devices,[22] antenna,[23] etc.[24] Interestingly, Ga-based metal alloys such as eutectic gallium-indium (EGaIn), gallium-indium-tin (Galinstan), gallium-indium-tin-zinc, etc. are worth noted for their high fluidity and low viscosity. However, EGaIn has shown to be the most preferred LM alloy in terms of its higher thermal conductivity (26.6 W m^{-1} K^{-1}) and electrical conductivity (3.4×10^6 $S.m^{-1}$), low melting point (15.5^oC), non-toxicity, mechanical stability, and excellent biocompatibility in composites.[25] A recent report by Pan et al. demonstrated improved dielectric breakdown strength for the PDMS (polydimethylsiloxane) composites upon LM insertion; however, at the cost of decreased mechanical performance.[26] A further drop in mechanical responses was observed when Bartlett et al. employed higher volume percent (vol% ~50) of LM in PDMS, eventually resulting in an inclusion modulus of 320 kPa.[27] The resulting hybrid elastic material was judiciously utilized for the fabrication of a light-emitting system in which the elastomeric composites were performing as stretchable electrical conducing materials. It is evident from recent investigations that LM offers remarkable compatibility in PDMS and yields ameliorated thermal and electrical properties at the expense of mechanical strength.[28] PDMS-based matrix possesses poor base strength in gel/liquid phases, rendering poor performance in terms of commercial usages. A viable commercial alternative would be an elastomer with high base strength that retains significant mechanical, electrical, and thermal properties upon mixing. Consequently, natural rubber (NR) holds an edge and is often regarded as a promising matrix for LM and other additives owing to its natural origin, superior mechanical strength, stress-induced crystallization, flex-fatigue resistance, tear-resistance, and low-temperature flexibility. Undoubtedly, NR finds itself irreplaceable in terms of a plethora of applications and is used in over 40,000 products worldwide that include car tires, aero tires, household appliances, surgical gloves, and numerous other medical devices.[29] Furthermore, inherent biocompatibility attributed to the fact that NR can stimulate angiogenesis, cellular adhesion, and repair tissue damage, contributed to significant commercial exploitation in diaphragms, blood bottles, cuff coils, pacifiers, and drug delivery systems.[30] To facilitate LM dispersion in PDMS-based elastomers, various methods were followed, for example, ultrasonic irradiation,[31] flow focusing in PDMS microchannels,[32] acoustic setups (piezoelectric transducer).[33] However, in these processes mentioned, only low molecular weight polymers can be mixed. On some occasions, solutions could also impart significant impurity or toxicity in the final product. Therefore, solution mixing and emulsification often require a specialized chemical condition to achieve high-quality composites.[34-35]

Herein, for the first time, we successfully developed liquid metal-embedded natural elastomer prototypes by standard rubber processing and vulcanization methods. To fabricate a liquid metal-solid rubber composite, a conventional two-roll mixing method was employed, followed by compression molding to develop cross-linked rubber sheets. Two-roll milling involves shear mixing of substrates using two rotating rollers, followed by mastication (scission of elastomeric chains). This investigation focuses on the influence of liquid metal (LM) EGaIn on the resulting rubber-composites' processability and physico-mechanical properties.

Relying on the above facts, the main objective of the proposed study is to devise a unique protocol towards designing LM (EGaIn)-NR-based binary composites using a standardized protocol with industrial yield and precision, eventually eliminating the obstacles faced by solution mixing-based methodologies. The mechanical and dielectric properties of the composites were critically investigated with reference to existing models. With this simple yet efficient protocol, we were able to embed liquid metal alloy droplets in soft, stretchable rubber to design conducting elastomers that might open up new frontiers in smart material engineering, emphasizing soft robotics and stretchable sensors for robotic devices.

2. EXPERIMENTAL

2.1 Materials

The natural rubber (NR) used in this study was Standard Vietnam Rubber (SVR-10). For the curing of NR, an organic peroxide (dicumyl peroxide, 99% pure DCP, Sigma-Aldrich) was utilized. The composition of liquid metal (LM) EGaIn was 75.5% gallium (99.99%) and 24.5% indium (99.99%) and was also procured from Sigma Aldrich Chemicals. Although no substantial data were found for acute toxicity of GaIn, CRC handbook revealed that the components of the alloy have low orders of toxicity.

2.2 Composite Fabrication

The rubber-metal alloy composites were fabricated by employing a conventional two-roll milling (Polymix 110L, size: 203 × 102 mm^2, Servitech GmbH, Wustermark, Germany). Each mixing was performed at room temperature with a friction ratio of 1:1.2 between the front and back rolls. The concentration of the filler is expressed in (weight) parts per hundred rubber (phr). Briefly, NR was masticated for 2 min. Mastication is an important step for the comounding of natural rubber. By this mastication process, the macromolecular chains of polyisoprene are fragmented into shorter

chains, resulting in a less viscous material which enables further incorporation of other rubber ingredients in the semisolid raw natural rubber. The addition of the LM was done by pouring the LM directly onto the nipgap of the two-roll. To avoid any splash during mixing the addition of LM was performed very slowly and the total time allotted for this step was 30 min. Afterwards, the curing agent DCP was mixed with the composite. The formulations of different batches are shown in Table 1.

Following the batch preparation, curing studies were performed using 5.5 g of the compounded samples. For this purpose, a moving die rheometer (Scarabaeus SIS-V50, Components & Machines e.U, Mauerbach, Austria) was used under the isothermal condition at 150°C for 1 hour. The optimum curing times (t_{90}) were measured, and samples were cured for the specified time by a hot press (Fortune Holland, Model TP 400) at 150°C. Sample sheets were kept for 24 hours at room temperature for further maturation. The sample fabrication process is schematically illustrated in the Fig. 1.

Table 1. various formulations of NR-LM composites

Sample*	**NR**	**EGaIn (LM) (phr)**	**DCP (phr)**
1 (NR-LM_0)	100	0	-
2 (NR-$LM_{12.5}$)	100	12.5	2
3 (NR-LM_{25})	100	25	2
4(NR-LM_{50})	100	50	2

*Concentrations are expressed in phr (parts per hundred of rubber by weight).

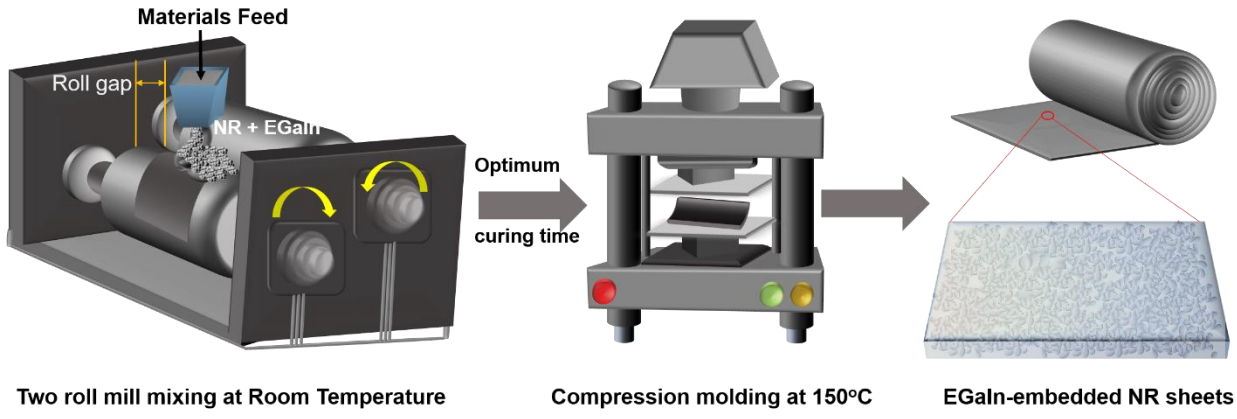

Figure 1. Schematic illustration of the processes involving LM-NR composite fabrication by two-roll mill mixing and compression molding. NR was masticated for 2 minutes in a two-roll mixing mill at room temperature following the 30 minutes mixing of LM and at the last curative. Finally,

the elastomeric LM-embedded NR sheet was prepared following the hot pressing of an uncured sample.

2.3 Characterization

Electron Microscopy. Surface morphologies and overall dispersion of LM droplets into the NR matrices were observed with a field emission scanning electron microscope (SEM; Zeiss NON40, Carl Zeiss Microscopy GmbH, Oberkochen, Germany). An ultramicrotome was used to cut the samples at -160°C. A custom-made stretching setup was integrated into the FESEM to accomplish the in situ stretching. A specified dimension of 3 mm ×1 mm specimen was clamped onto the device prior to stretching. Beforehand, samples were coated with a thin layer of carbon (10 nm to 20 nm) to prevent the charging of the specimen in the electron beam. The shape and composition of the LM droplets were observed with TEM (Libra200, Carl Zeiss Microscopy GmbH, Oberkochen, Germany) equipped with an omega-type energy filter and operated at the acceleration voltage of 200 kV. The elemental maps were generated from a series of energy-filtered TEM images using the 3-windows method.[35]

Tensile Measurements: The tensile measurements were conducted according to ISO[36] rules using a Zwick 1456 tensile tester (Zwick Roell GmbH, Ulm, Germany) fitted with optical strain sensors. Uniaxial tensile cyclic experiments were carried out by stretching the samples with different strains of 50 %, 100 %, and 200 % (three cycles each), and finally stretched up to failure.

Tear Fatigue Analysis: Fracture mechanical behavior of the NR-LM composites was investigated to evaluate the microcrack propagation resistance of the composites in contrast to the unfilled NR vulcanizate. A COESFELD Tear and Fatigue Analyzer (TFA, Darmstadt (G)) was used for the study. The dimension of the 'pure shear' specimen was (40 mm×4 mm×1 mm). A preloading force with 1 N under sinusoidal loading conditions with 2 Hz frequency was used for the test. The measurement was performed at room temperature. According to Paris and Erdogan, the stable crack growth rate (da/dn) depends on the tearing energy (T) following a power law equation,[37]

$$\frac{da}{dn} = \beta T^m \qquad (1)$$

where β and m are material constants, a and n denote the crack length and number of cycles, respectively. The above equation is valid in the stable crack growth region where ($T_1 \leq T \leq T_c$). T_1 represents the corresponding tearing energy where the crack is just started to propagate, and T_c

is the critical tearing energy, and after that, the crack propagates catastrophically. The tearing energy *T* can be calculated by the following equation

$$T = w \cdot L \qquad (2)$$

where *w* is the strain energy density which is calculated automatically by the instrument, and *L* (distance between the clamps) is the sample length. For the measurement of crack length, '*a'* an optical measurement unit with a fitted CCD-video camera is used. The camera is able to move along the crack canter, and the image can be processed internally to give the value of crack length.

Dielectric measurement: Dielectric measurements were performed using HP 4284A LCR meter with short wire connected metal conductors. To avoid wrinkles on the specimen, different geometrical conductors with flat surfaces were used in the measurements. These measurements were conducted exclusively in parallel circuit mode where conductor edge correction was taken into account.[20] Details of these dielectric measurements are provided in the supporting information.

Thermal Conductivity Measurement: Thermal conductivities of the pristine NR and NR-LMs were conducted on a Laser Flash apparatus coupled with infrared sensor technology in a vacuum (LFA 467 Micro flash) and at room temperature with a nitrogen atmosphere. The typical sample thickness and diameter for the measurement were 11 mm and 9 mm, respectively. The surface of a plane parallel sample was heated using a short energy light pulse. The resulting temperature increment on the rear face was measured by an infrared detector. Thermal conductivity was derived from the calculated diffusivity (α) and specific heat (c_p), according to the following equation:

$$\lambda(T) = \alpha(T).\, c_p(T).\, \rho(T) \qquad (3)$$

where ρ is the density of the specimen.

Differential Scanning Calorimetry (DSC): DSC measurements were carried out using Q1000 (TA Instruments, USA) calorimeter. An autosampler was coupled with the instrument, and a heating rate of 10^{o}C/min was applied in the temperature range of -50 to +150^{o}C.

3. RESULTS AND DISCUSSION

The rheometric response curves of NR and NR-LM composites are shown in Fig. 2a. The torque-time curves were nearly identical for all the specimens and indicated a steady increment in torque values upon the addition of curatives (dicumyl peroxide, DCP). However, the incorporation of LM

did not necessarily lead to any change in torque response or optimum cure time (t_{c90}). It is noted that the interaction between DCP and unsaturated rubber chains was unperturbed by the addition of LM. However, with an increase in LM loading, a slight decrease in torque value was observed owing to the softening of the resulting rubber composites. Initially, a sulfur-based curing package was considered as the first attempt to cure the NR-LM composites. However, curing was not possible in the presence of LM as it somehow inhibited the formation of active sulfur curing precursors. The ongoing observation on this particularly interesting aspect of vulcanization chemistry for rubbers in presence of LM will be separately communicated.

The mechanical behavior of the sample NR-LM_{50} was investigated under tensile loading. Fig. 2b demonstrates the representative uniaxial stress-strain curves for NR-LM_{50} and compared to that of unsubstituted control (NR-LM_0). It was observed that the NR-LM_{50} was stretchable up to a staggering ~ 650% strain, and there was no loss or gain of stretchability (elongation at break) as compared to pure NR due to uniform mechanical deformation of LM and NR under uniaxial stretching. The elongation of LM droplets encapsulated in NR along the stretching direction could also manifest in exceptional tensile toughness of NR-LM_{50}. Generally, an overall reduction in stretchability is a common phenomenon for rigid particle-substituted soft matrix owing to non-uniform mechanical deformation of the soft substrate with respect to rigid inclusions. The addition of LM in rubber may not be compared to that of the softener or plasticizers. In principle, after the addition of plasticizers, the stiffness or moduli of the rubber composites have been shown to decrease. In the present case, however, the effect is turned out to be the opposite. The influence of stiffness on the LM inclusions of the resulting composites was studied by measuring the 100 % modulus (i.e., stress value at 100 % elongation). It is observed from Fig. 2c that, with an increase

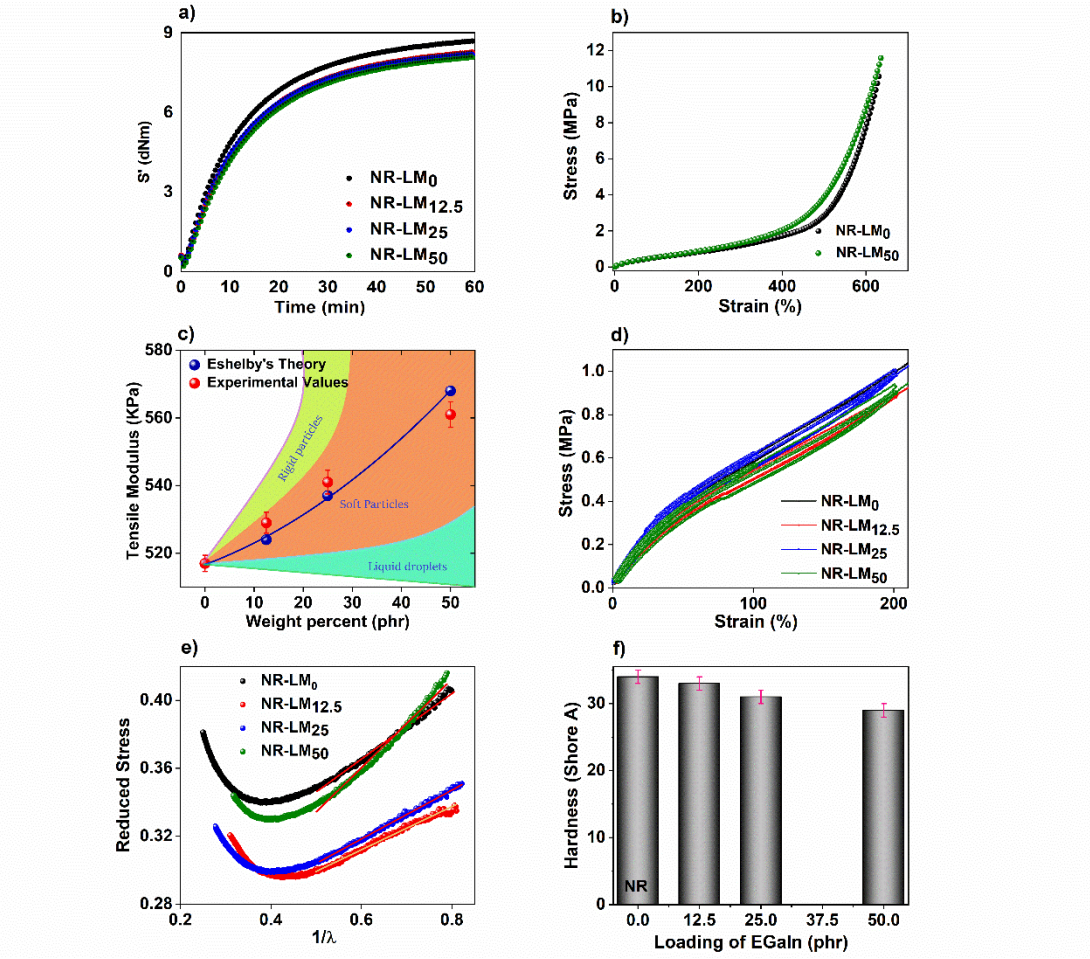

Figure 2. Mechanical properties of LM-loaded NR composites (0, 12.5, 25 and 50 phr LM): a) torque-time curves and rheometric analysis, b) representative stress-strain curves for NR and 50 phr LM-loaded NR composites (NR-LM_{50}), c) tensile moduli at 100% elongation vs. wt% (phr) of LM (the dashed line shows the Eshelby's prediction illustrating an increase in tensile moduli with soft particle inclusion), d) Cyclic loading-unloading and analysis of hysteresis loss, e) Mooney-Rivlin plots (reduced stress vs. extension ratio) of different composites, and f) comparison of the hardness of different NR-LM composites.

in LM-loading from 0 to 50 phr, modulus at 100 % elongation was increased from ~530 KPa to ~570 KPa. The resulting composite is expected to possess an infinite bulk modulus (K) as the components NR and LM are assumed to be virtually incompressible:[27]

$$K_{elastomer} = K_{liquid\ metal} = K_{composite} = \infty \qquad (4)$$

Therefore, considering the incompressible elastic inclusion in an incompressible elastic matrix, theoretical moduli of the resulting composites can be predicted by Eshelby's approach. According to this model, the modulus of the composite (E_c) can be calculated by the following equation,[38-39]

$$E_c = E_p \frac{1+{}^{2\,E_i}/_{3\,E_p}}{\left({}^{2}/_{3}-{}^{5\,\varphi}/_{3}\right){}^{E_i}/_{E_p}+\left(1+{}^{5\,\varphi}/_{3}\right)} \quad (5)$$

where E_i and E_p are the moduli of the inclusion and the polymer matrix, respectively. The volume fraction of the included substance is denoted by φ. The modulus calculation of a liquid particle is critical and was demonstrated by Style et al.[38] According to the theory, if incorporated liquid droplet radii are larger than the elasto-capillary scale, the resulting composite becomes more compliant and, therefore, results in significant strain hardening. From morphological analysis (discussed later), it was evident that the droplet sizes are in submicron ranges, thus, both experimental and theoretical calculations confirmed the stiffening of the compliant solid matrix. It is worth noting that for both the sample NR-$LM_{12.5}$ and NR-LM_{25} (with 12.5 and 25 phr), experimental moduli were very close to that of the theoretically predicted values. However, a slight mismatch between the two was observed for the NR-LM_{50} (Fig. 2c). The coalescence of LM droplets by the intramolecular attraction and subsequent increment in droplet dimension in NR-LM_{50} could plummet the modulus value to a lower one than that of predicted modules. Additionally, surface tension (γ) at the solid-liquid interface could also play a crucial role. Surface tension maintains the droplets in a spherical shape, which resists the external forces. Bartlett et al. calculated the value of Ei as ~ 129 KPa following a relation between Ei with γ, radius of the droplets (R) and modulus of the polymer (E_p) which are experimentally determined.[27]

In Fig. 2d, cyclic stress-strain curves of various composites at different strains (50, 100, and 200 %) are shown to demonstrate hysteresis behavior.[40] After the completion of each cycle, it was observed that the hysteresis loss effect was marginal as compared to pure unsubstituted NR. The friction in the network has turned out to be insignificant following the addition of elastic LM droplets; hence, the permanent residual strain of the composites turned out to be negligible and

eventually comparable to that of pure NR. It indicates that the elasticity of NR is almost unaffected even after the 50 phr EGaIn loading (NR-LM_{50}).

Mooney-Rivlin curves were derived for NR vulcanizate and LM-loaded NR composites (Fig. 2e). From the plots of Mooney Rivlin equation, the cross-linking density values was evaluated (see the supporting information) and are listed in Table 2. These values followed the same trend as the respective ultimate torque values in the rheometric study. An inverse correlation between cross-linking density and LM loading could possibly be associated with the inclusion of LM that could hinder the polymer chains approaching each other, thus preventing the chemical cross-linking between two chains. Fig. 2f shows the hardness values of different composites. With the addition of 12.5 phr LM, there were no measurable changes in hardness observed. Nevertheless, with the addition of 25 and 50 phr LM, a slight decrease in Shore A hardness was detected. Precisely, a reduction of 5 units of Shore A hardness was achieved following the inclusion of 50 phr LM into the NR matrix. Generally, upon inclusion of fluid phases or soft particles into the matrix, reduction in intermolecular friction occurs commonly attributed to the cushioning effect. This decrease in frictional forces is further reflected in the hardness values.[41]

Table 2. Cross-linking densities by the phenomenological Mooney-Rivlin model

Sample	**Intercept (C_1)**	**CLD (mol/cm^3)**
NR-LM_0	0.124	5.03×10^{-5}
NR-$LM_{12.5}$	0.117	4.75×10^{-5}
NR-LM_{25}	0.116	4.68×10^{-5}
NR-LM_{50}	0.102	4.12×10^{-5}

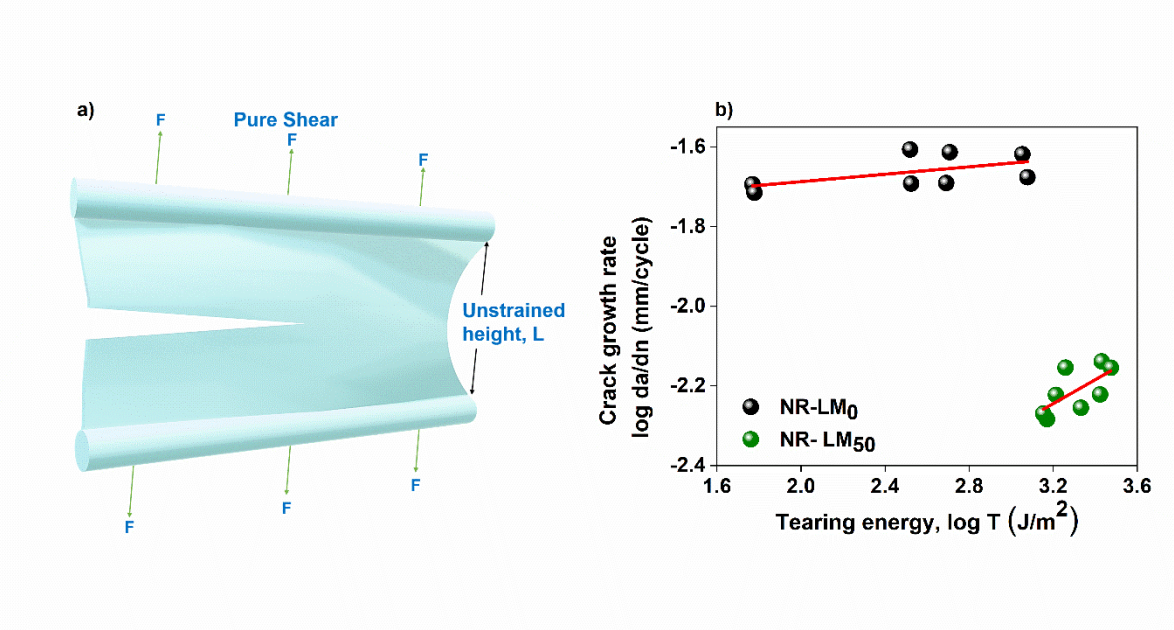

Figure 3. a) Schematic of the pure shear rubber specimen for tear fatigue analysis, b) the fracture property comparison between unfilled NR and 50 phr EGaIn-loaded NR vulcanizate (NR-LM_{50}) are shown in terms of Paris plot (crack growth rate vs. tearing energy).

Fig. 3a illustrates a pure shear specimen used in the tear fatigue analysis, and Fig 3b indicates significantly lower fatigue crack growth rate with substantially higher tearing energy for the LM-embedded NR composites compared to that of unsubstituted NR vulcanizate. A closer look at Fig. 3b reveals that tearing energy required for the initiation of crack growth of NR-LM_{50} was enhanced by nearly 6 times (~ 330 to ~ 2140 J/m^2). Conversely, a reduction in the initial crack growth rate of up to 4 times was achieved following the LM-inclusion. It has been shown that improved fracture mechanical properties are the hallmark of rigid filler-based elastomeric composites for

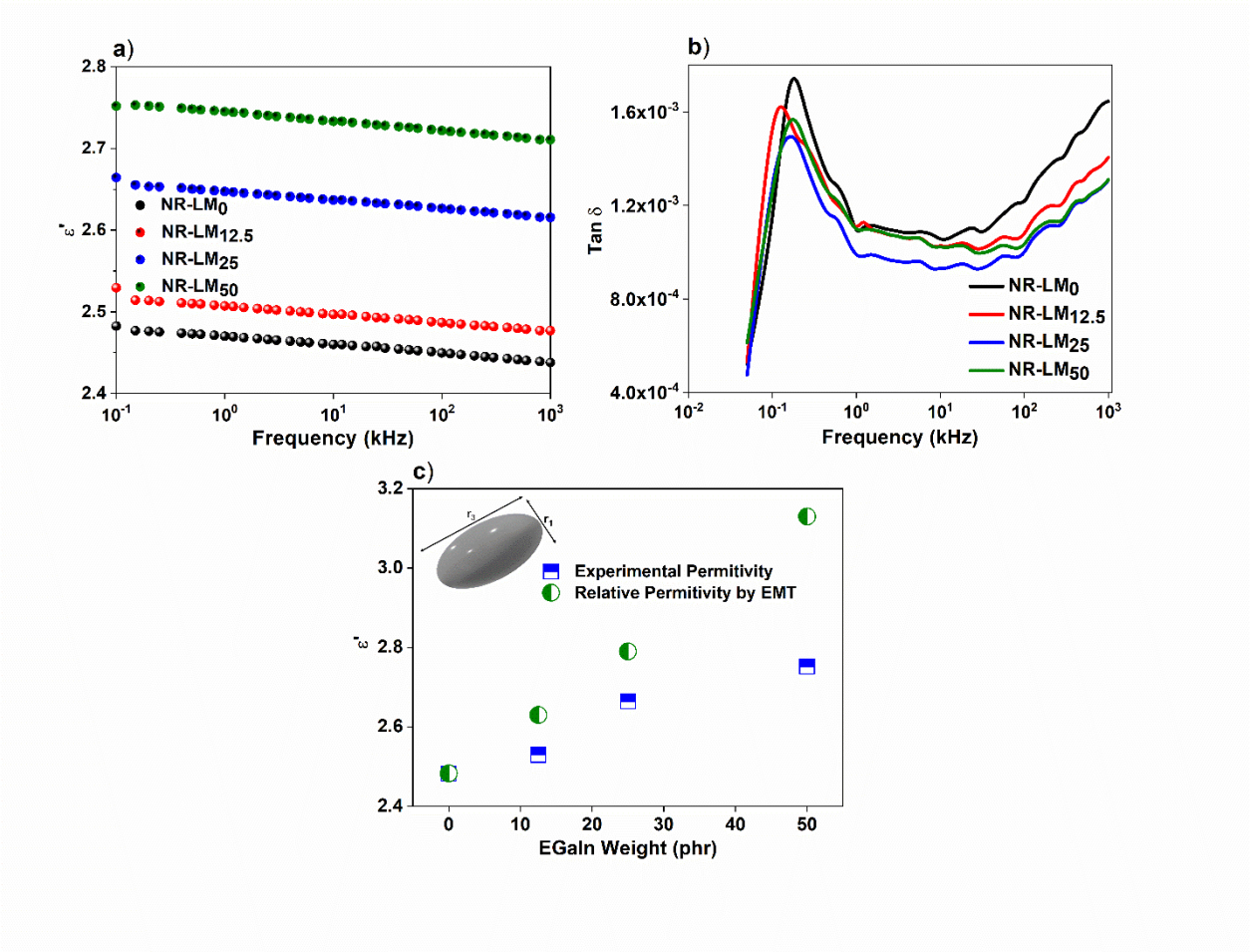

Figure 4. Dielectric properties of NR vulcanizate and LM-loaded NR (12.5, 25 and 50 phr of EGaIn) composites: a) dielectric constant vs. frequency, b) dissipation factor vs frequency c) dielectric constant at 100 Hz (from experimental and effective medium theory) vs. weight of the LM in phr. All dielectric studies were performed at 104 kPa.

which, tear typically propagates through the longitudinal direction.[42] Rigid filler composites are characterized by larger localized strain zones and are propagated from the crack tip leading to a higher energy dissipation.[43] However, fluidic inclusions, as is the case for LMs, are known to have additional mechanisms of crack dissolution due to the deflection of tear, adaptive movement of crack, high energy dissipation, and destruction of crack tips. According to Cook and Gordon, depending upon the interfacial energy analogy between the LM and NR, the crack initiated perpendicular to the original crack eventually prevents the tearing of the whole specimen.[44] Furthermore, unlike rigid particles, liquid inclusions deform uniformly within the surrounding elastomeric medium. Additionally, small external impacts and the presence of local strain fields

often lead to droplet elongation and subsequent dynamic deformation far from the crack formation region.[43] These factors account for the improved fracture mechanical properties of the NR-LM_{50} vulcanizate. Notably for the propagation of the crack, the required total energy should be higher than the intrinsic strength of the molecular structure. Reason are contributions to the crack propagation energy from the viscoelastic deformations of the rubber in front of the propagating crack tip.[45] Therefore, the crack propagation energy is determined by the bond-breaking processes at the crack tip and, additionally, by the viscoelastic energy dissipation in front of the crack tip. The last part even occurs very far from the crack tip and plays an essential role in fracture behaviors of soft rubbers. A dielectric material with an insulating character gets polarized when subjected to an external electric field, resulting in the redistribution of free charge carriers slightly shifted from the equilibrium position. This phenomenon is defined as dielectric polarization, mainly caused by the charge redistribution that weakens the external electric field. The net dipole at a specific location is the summation of all charge displacement vectors from the superposition principle. Fig. 4a and 4b illustrate the variation of the dielectric constants and the dissipation factors with the frequency for both the pristine and LM-substituted NRs.

It is apparent that characteristic dielectric responses are intrinsically similar, and dielectric constants decrease marginally with the frequency in a linear fashion. For NR-LM_{50}, the dielectric constant is increased to 2.75 at 100 Hz, an impressive 11% increment in ε' compared to that of pristine NR (2.48). This enhancement can be explained in terms of interfacial polarization in the NR-LM composites.[46]

With the introduction of a new phase (LM) in the NR matrix, the interfacial or space-charge polarization effect comes into play. Characteristic to multiphase polymeric systems, Maxwell-Wagner interfacial polarization is primarily responsible for the dielectric behavior in these systems where orientation and dipolar contribution to polarization may not be prevalent. Also, with the increase in LM loading, an externally applied electrical field releases the charges accumulated on the NR-LM interfaces and effectively facilitates migration between the phases, forming a few dipoles.[47] This can be expressed by the following relation:

$$\varepsilon'(\omega) = \varepsilon_\infty + \frac{(\varepsilon_s - \varepsilon_\infty)}{1+\omega^2\tau^2} \qquad (6)$$

where ω is the angular frequency, τ is the relaxation time which is inverse of the frequency at the maximum dielectric loss, ε_∞ and ε_s are the real part of dielectric values at high and low frequencies and are defined by

$$\varepsilon_\infty = \frac{1}{\frac{\sum_i \vartheta_i}{\varepsilon'_i}} \quad (7)$$

$$\varepsilon_s = \frac{\frac{\sum_i \vartheta_i \varepsilon'_i}{{\sigma_i}^2}}{\left(\frac{\sum_i \vartheta_i}{\sigma_i}\right)^2} \quad (8)$$

σ_i, ϑ_i, ε'_i are the conductivity, volume fraction and permittivity of the individual components, respectively.[47]

Depending on the microstructure, the dielectric properties can be elucidated using Effective Medium Theory (EMT). As the LM droplets embedded in the NR matrix were ellipsoidal in shape, relative permittivity can be evaluated using the following relation by Nan et al.,[48]

$$\varepsilon_r = \varepsilon_m \frac{1+\left\{\frac{1-L_{11}}{L_{11}}\left(\langle 1-cos^2\theta\rangle\right)+\frac{1-L_{33}}{L_{33}}\left(\langle cos^2\theta\rangle\right)\right\}\varphi}{1-\varphi} \quad (9)$$

where ε_m is matrix permittivity, φ is the volume fraction of LM inclusion, θ is the angle between the axis of the permittivity and the principal axis. The value of $\langle cos^2\theta\rangle$ is $\frac{1}{3}$ for the randomly oriented ellipsoids. L_{11} and L_{33} are the factors dependent on the shape of the particle and can be calculated as:

$$L_{11} = \frac{p^2}{2(p^2-1)} - \frac{p}{2(p^2-1)^{3/2}} cosh^{-1}p \; for \; p > 1 \quad (10)$$

$$L_{33} = 1 - 2\,L_{11} \quad (11)$$

where $p = \frac{r_3}{r_1}$ = 1.49

For the NR-$LM_{12.5}$ and NR-LM_{25}, experimental data do not deviate significantly from the theoretical data. However, with the addition of 50 phr of LM, the spread between the theoretically predicted value with that of the experiment was much higher (Fig. 4c). Because of the coalescence of liquid droplets in NR-LM_{50} loading, the geometry of the ellipsoids might have transformed into

irregular shapes. Thus, the aspect ratio has been reduced to some extent. The related discussion is addressed further in the proceeding microscopy section. With coalescence, as the number of LM droplets decreases, the interface volumes and the resulting interfacial polarization could also be depleted, resulting in an overall reduction in dielectric properties.

The dissipation factor (ε'') originates from the inability of the polarization process to follow the rate of change in the oscillating applied electric field and is related to the relaxation modes of the system. A modest loss of dissipation factor is generally attributed to the movement of polymer chains and reorientation of the segments. The inverse of the frequency at the maximum loss is expressed in terms of relaxation time and is denoted by τ.[49] It depends on the factors like Maxwell–Wagner–Sillars effect (MW), electric dipole polarization (D), and leakage conductivity loss (DC).[50]

$$\varepsilon'' = \varepsilon_{MW} + \varepsilon_D + \varepsilon_{DC} \quad (12)$$

Fig. 4b revealed that NR-LM composites possessed lower dissipation factors and arguably better charge storage properties than the pristine NR.

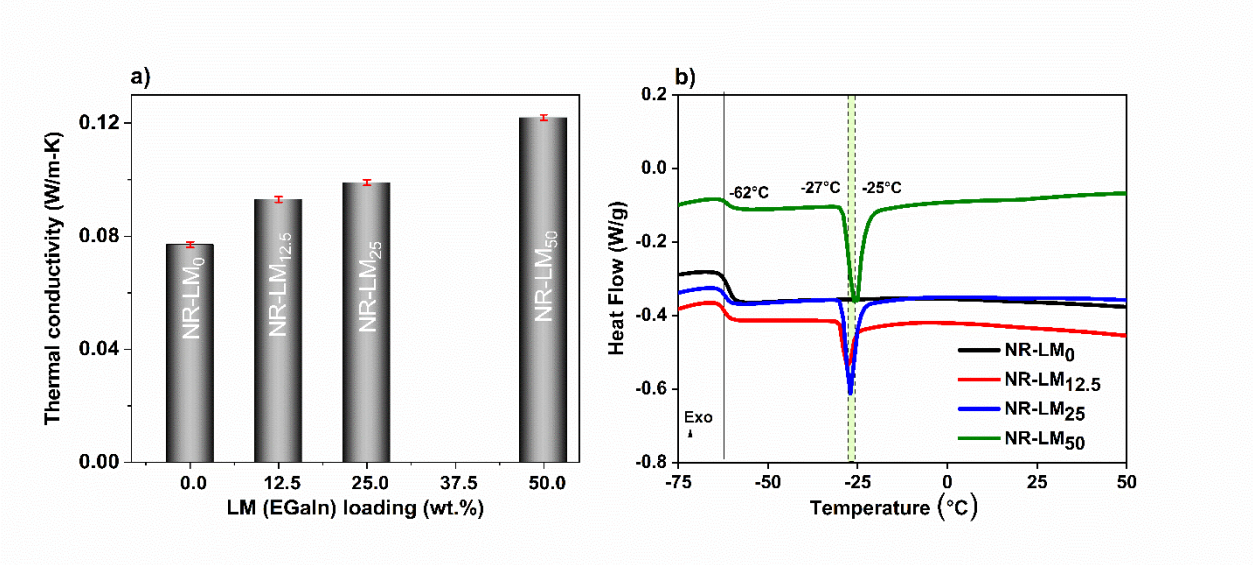

Figure 5. a) Thermal conductivities of various NR-LM composites are shown as functions of weight percentage of LM (phr), and b) Differential scanning calorimetry (heat flow vs temperature) analyses of the NR-LM composites.

Soft rubber materials with lower elastic modulus generally possess lower thermal conductivity due to phonon transport dynamics.[51] Elastic modulus (E) is proportional to the thermal conductivity (k) and can be expressed as following,[52-53]

$$k = \left(\frac{E}{\rho}\right)^{\frac{1}{2}}\left(\frac{C_v l}{3}\right) \quad (13)$$

where, ρ is the density, C_v is the volumetric heat capacity, and the phonon average mean free path is l. Generally, rubber composites offer poor thermal conductivities where phonon scattering is caused by spatial fluctuations (in sound velocity), and pronounced transverse mode scattering, which is more than the longitudinal ones.[54] In the present case, the advantage of liquid metal inclusion in NR leans on the fact that LM droplets are composed of metallic free electrons that can dominate the Newton-Laplace effect.[54] Accordingly, to this effect, k increases with an increase in elastic modulus. Here, an increased k value can be achieved without an increase in elastic moduli of the resulting composite. Although with secondary electronic conduction, the expected increase of the k value is less but significant in the present case. Evidently, a systematic increment in thermal conductivity was reported with increased LM-loading (Fig. 5a). Previously, Bartlett et al. reported that PDMS with 50 vol% of GaIn (~310 phr) offered an impressive 25-times and 50-times increment in k value under the normal and stretched conditions, respectively. In our case, however, the addition of only 50 phr of EGaIn (~8 vol%) in NR can contribute an outstanding ~58% jump in k value as compared to that of pristine NR.

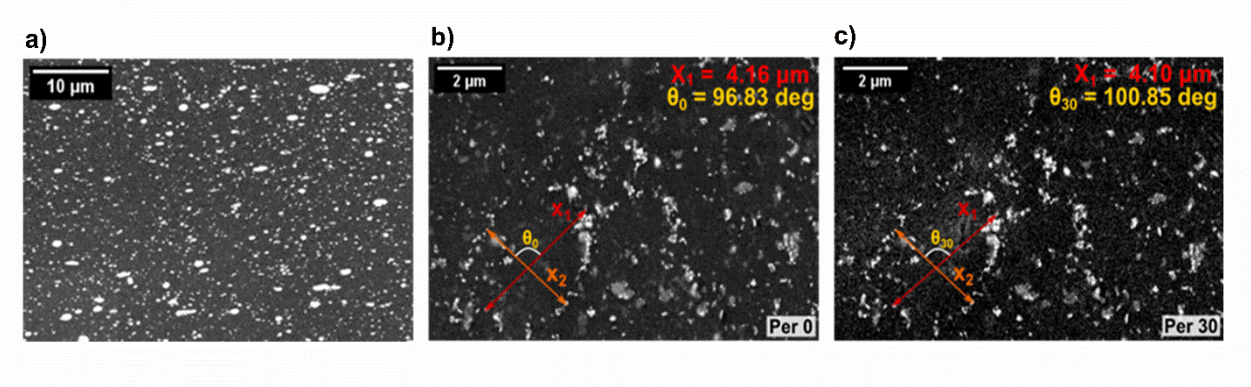

Figure 6. Scanning electron microscopy (SEM) images of NR-LM_{50}, a) Distribution of Ga-In in the elastomer matrix, b) In-situ stretching experiment in SEM at 0% elongation, and c) at 30% elongation.

The DSC curves of pristine NR and NR-LM composites are shown in Fig. 5b. As NR is an amorphous material, the corresponding glass transition temperature (T_g) was found to be around -62°, with the addition of LM, the T_g was not altered. With the addition of LM in the NR matrix, distinctive melting peaks emerged owing to the melting of LM in the matrix. However, melting

temperatures appeared to be slightly shifted towards higher regime with higher loading of LM (-27°C to -25°C). Kumar et al. formerly reported a change in melting temperature of Ga by altering the particle size (micron to sub-micron), by means of sonicating molten Ga.[54] The authors observed an approximate 2K drop in melting point while the diameter of Ga was larger than 0.45 µm.[54] Fig. 5b reports a similar variation in melting point peaks owing to the change in particle/droplet size, arguably derived from a similar analogy. Continuous friction between the rubber chains during mastication and with the action of the front and back rolls, the LM particles appeared to have dispersed within the NR matrix in reduced sizes. The melting temperature

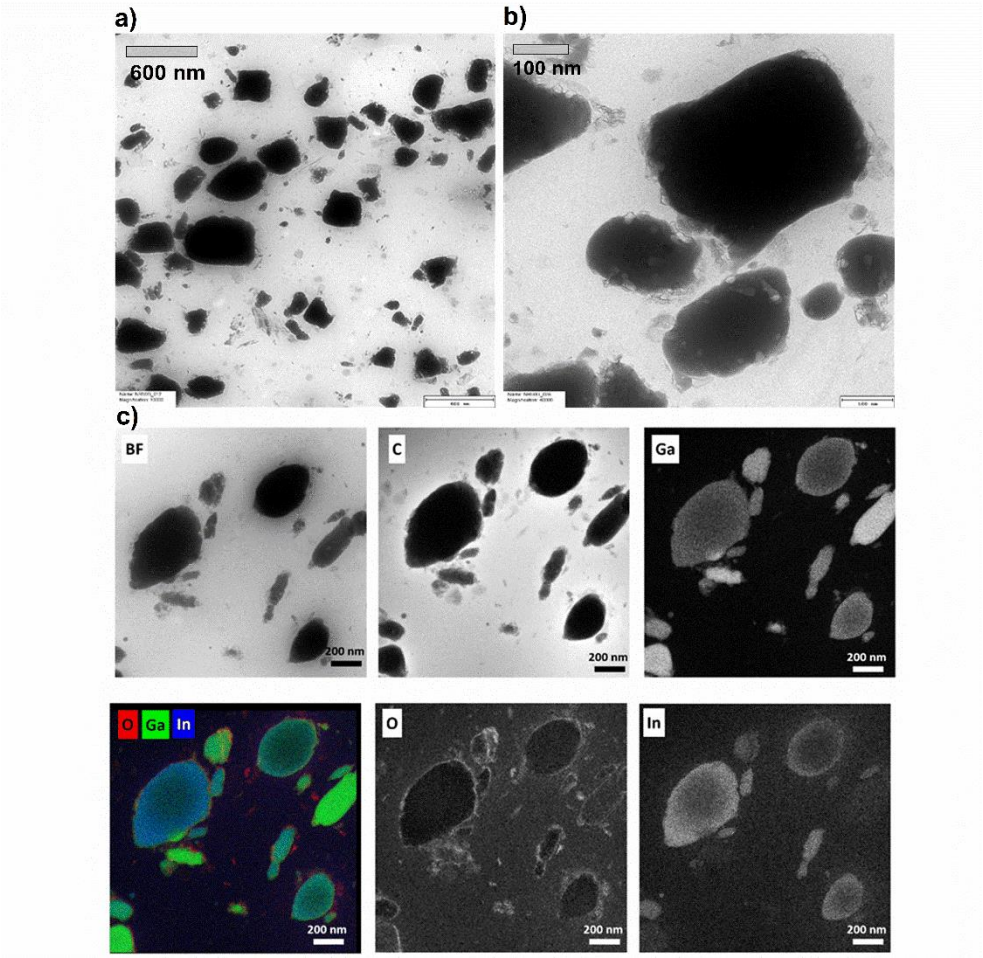

Figure. 7. a) and b) transmission electron microscopy images of 50 phr LM filled NR, c) Bright field (BF) TEM image and elemental maps of NR-LM_{50}. Bottom left represents the color overlay of O, In, Ga elemental maps.

of pure GaIn is 15.5°C[23]. However, with the addition of 12.5 phr GaIn in the rubber matrix, the endotherm of melting was shifted to a lower temperature due to the reduced sizes of GaIn (in the

submicron range). With the addition of 25 and 50 phr of GaIn, the melting endotherms were found out to be at -27°C and -25°C, respectively. This small increment was attributed to the coalescence of a fraction of LM droplets in higher loads of Ga in the NR matrix. To assess the dispersion and distribution of LM in the NR matrix, a detailed morphological characterization was performed using scanning and transmission electron microscopy images. It was realized that the shape, size, and distribution of LM have a significant impact on the mechanical and other physical properties of resulting rubber composites. The SEM micrographs from Fig. 6a revealed a disordered yet uniform distribution of the LM particles in the NR matrix. Furthermore, it was evident that the shapes of the microparticle droplets are not spherical; rather, ellipsoidal shapes were prevalent at the submicron level. This morphological finding is in close agreement with the conclusion derived from DSC studies. The structural changes of the particles inside the elastomer matrix upon stretching would possibly extract more insight into the mechanism and morphological correlation. Subsequent changes can be understood by coupling in-situ stretching with SEM. The SEM images acquired during the quantitative changes upon stretching are shown in Fig. 6b and 6c. We observed that upon stretching, the shapes of the particles did not alter at all, even after 30% stretching, indicating the hard particle-like nature of the micro droplets rather than liquid droplet configuration otherwise expected. An elliptical assembly of the micro droplets in the sub-figures of 6b and 6c has been spotted. A close proximate has been assigned for the major (X_1) and minor (X_2) axis. The values of X_1, X_2, and θ (the angle between X_1 and X_2) document the outcome. Remarkably, the changes in the values of X_1 and X_2 were negligible and came under the error margin. X_1 and X_2 vary between 4.13 ± 0.03 and 3.16 ± 0.03 µm, respectively. However, due to the compressive strain perpendicular to the direction of stretching, a few minor changes have been spotted. The angle theta changed from 96.83 deg to 100.85 deg; this nominal change can be attributed to the elongation. To sum up, morphological anomalies under stretching condition can be attributed to two key factors based on our documentation: first, the solid elastic membrane like behavior of Ga_2O_3 can withstand the elongation, and the interface may deform, but that negligible deformation is possibly insufficient to deform the microdroplets; second, the excess stress in the matrix releases upon forming cracks, so the local changes are negligible. Some wider cracks have been spotted on a larger scale. The effective strain in the region of interest may change infinitesimally owing to the wider cracks spotted on a larger scale and the stress relaxation (as a function of time). The presence of an oxide layer has been experimentally documented in TEM color mapping and discussed in the proceeding section.

TEM micrographs revealed that the shape of the LM particles is largely inhomogeneous, and therefore, a mixed morphological appearance was more prevalent. The particle size distribution analyses indicated a wide distribution of LM ranging from ~ 50 nm to ~ 500 nm. As discussed in the preceding section, the surface of GaIn could be partially oxidized by air and/or by the presence of peroxide used in the cross-linking of NR. This facilitates the formation of a thin layer of Ga_2O_3 on the LM droplets. Owing to the lower surface tension of metal oxide, it would manifest itself more like a solid elastic membrane (critical surface stress ~ 0.5 N/m).[25] Furthermore, the outer oxide layer could likely stabilize the particle morphology and eventually facilitate the compatibility between LM and NR.

TEM images (Fig. 7a-b) indicated a wide distribution of LM particles in different sizes and forms. Relatively large and round LM droplets could be spotted with that relatively smaller particles of edgy shape. The elemental maps (Fig. 7c) revealed that the microdroplets are not a homogeneous mixture of Ga and In, but a variation of Ga:In ratio could actually be evident. This phenomenon is also reported elasewhere.[33, 55] We also noticed that the extent of phase separation depends on the sample preparation for the microscopic images. Most probably, when the sample was cryo-microtomed, the phase separation was more prominent.

Furthermore, oxygen is abundant in some discrete zones, which could have originated from peroxide-based cross-linking agents. Moreover, a thin oxygen-rich shell around the particles was observed in conjunction with the observation from in-situ stretch couple SEM measurements. The aerial oxidation and presence of peroxide crosslinkers led to significant surface oxidation that could account for the stabilization of the droplets under strain.

4. CONCLUSION

Liquid metal embedded soft and highly stretchable elastomeric composites were successfully developed using a conventional rubber processing and vulcanization method for the first time. In this process, highly deformable liquid metal is fragmented and dispersed into submicron sizes within the NR matrix. An extraordinary improvement of the tear fatigue properties is noticed. The tearing energy of LM-embedded NR is enhanced up to ~6 times (330 to 2150 J/m^2), and nearly 4 times reduction in crack growth rate are achieved as compared with pure NR. The incorporation of 50 phr (8 vol %) EGaIn transformed the composite into a robust and ultra-stretchable (elongation at break ~ 650%) rubber composite with modulus in kilopascal range (~ 530-570 kPa at 100%

elongation). In terms of thermal conductivity, the value is shown to be increased up to 58% (0.077 to 0.122 W/m-K) as compared to pristine NR. Finally, SEM/TEM morphological investigation suggested a disordered, inhomogeneous distribution of the LM as hard nanospheres in the NR matrix ranging from 50 to 500 nm inclusion size. The controlled balance of soft material flexibility with increased tear resistance in NR-LM composites would eventually instigate significant practical impacts in soft electronics, biological devices, and soft robotics.

5. ACKNOWLEDGEMENT

The corresponding work is financially supported by The Deutsche Forschungsgemeinschaft (DFG, German Research Foundation) project ID 330167 – SPP 2100. A. Das thankfully acknowledges René Jurk for mechanical experiments and U. Reuter for specimen preparation for TEM and SEM.

G. H. acknowledges the DFG (German Research Foundation) project 380321452/GRK2430 for financial support.

Supporting Information: Experimental details on dielectric analysis and Mooney-Rivlin plot, photograph of the cured NR-LM composite.

REFERENCES

1. Whitesides, G. M., Soft robotics. *Angewandte Chemie International Edition* **2018,** *57* (16), 4258-4273.
2. De Falco, I.; Gerboni, G.; Cianchetti, M.; Menciassi, A., Design and fabrication of an elastomeric unit for soft modular robots in minimally invasive surgery. *Journal of visualized experiments: JoVE* **2015,** (105).
3. Cianchetti, M.; Laschi, C.; Menciassi, A.; Dario, P., Biomedical applications of soft robotics. *Nature Reviews Materials* **2018,** *3* (6), 143-153.
4. Bergbreiter, S.; Pister, K. S. In *Elastomer-based micromechanical energy storage system*, ASME International Mechanical Engineering Congress and Exposition, **2006**; pp 539-545.
5. Majidi, C.; Haataja, M.; Srolovitz, D., Analysis and design principles for shear-mode piezoelectric energy harvesting with ZnO nanoribbons. *Smart materials and structures* **2010,** *19* (5), 055027.
6. Patino, T.; Mestre, R.; Sanchez, S., Miniaturized soft bio-hybrid robotics: a step forward into healthcare applications. *Lab on a Chip* **2016,** *16* (19), 3626-3630.
7. Wong, W. S.; Chabinyc, M. L.; Ng, T.-N.; Salleo, A., Materials and novel patterning methods for flexible electronics. In *Flexible Electronics*, Springer: **2009**, pp 143-181.
8. Ashizawa, M.; Zheng, Y.; Tran, H.; Bao, Z., Intrinsically stretchable conjugated polymer semiconductors in field effect transistors. *Progress in Polymer Science* **2020,** *100*, 101181.
9. Muth, J. T.; Vogt, D. M.; Truby, R. L.; Mengüç, Y.; Kolesky, D. B.; Wood, R. J.; Lewis, J. A., Embedded 3D printing of strain sensors within highly stretchable elastomers. *Advanced materials* **2014,** *26* (36), 6307-6312.

10. Yun, G.; Tang, S.-Y.; Zhao, Q.; Zhang, Y.; Lu, H.; Yuan, D.; Sun, S.; Deng, L.; Dickey, M. D.; Li, W., Liquid metal composites with anisotropic and unconventional piezoconductivity. *Matter* **2020,** *3* (3), 824-841.
11. Kofod, G., Dielectric elastomer actuators. *Chemistry* **2001**.
12. Wang, J.; Yan, C.; Chee, K. J.; Lee, P. S., Highly stretchable and self-deformable alternating current electroluminescent devices. *Advanced Materials* **2015,** *27* (18), 2876-2882.
13. Niu, X.; Peng, S.; Liu, L.; Wen, W.; Sheng, P., Characterizing and patterning of PDMS-based conducting composites. *Advanced Materials* **2007,** *19* (18), 2682-2686.
14. Liu, H.; Zhang, L.; Yang, D.; Yu, Y.; Yao, L.; Tian, M., Mechanical, dielectric, and actuated strain of silicone elastomer filled with various types of TiO2. *Soft Materials* **2013,** *11* (3), 363-370.
15. Gallone, G.; Carpi, F.; De Rossi, D.; Levita, G.; Marchetti, A., Dielectric constant enhancement in a silicone elastomer filled with lead magnesium niobate–lead titanate. *Materials Science and Engineering: C* **2007,** *27* (1), 110-116.
16. Li, F.; Qi, L.; Yang, J.; Xu, M.; Luo, X.; Ma, D., Polyurethane/conducting carbon black composites: structure, electric conductivity, strain recovery behavior, and their relationships. *Journal of Applied Polymer Science* **2000,** *75* (1), 68-77.
17. Subramaniam, K.; Das, A.; Steinhauser, D.; Klüppel, M.; Heinrich, G., Effect of ionic liquid on dielectric, mechanical and dynamic mechanical properties of multi-walled carbon nanotubes/polychloroprene rubber composites. *European polymer journal* **2011,** *47* (12), 2234-2243.
18. Fu, S.-Y.; Feng, X.-Q.; Lauke, B.; Mai, Y.-W., Effects of particle size, particle/matrix interface adhesion and particle loading on mechanical properties of particulate–polymer composites. *Composites Part B: Engineering* **2008,** *39* (6), 933-961.
19. Johns, J.; Nakason, C., Dielectric properties of natural rubber/chitosan blends: Effects of blend ratio and compatibilization. *Journal of Non-Crystalline Solids* **2011,** *357* (7), 1816-1821.
20. Codrington, R. S. A dielectric properties of natural and synthetic rubber-sulphur compounds. University of British Columbia, **1948**.
21. Tang, S.-Y.; Khoshmanesh, K.; Sivan, V.; Petersen, P.; O'Mullane, A. P.; Abbott, D.; Mitchell, A.; Kalantar-Zadeh, K., Liquid metal enabled pump. *Proceedings of the National Academy of Sciences* **2014,** *111* (9), 3304-3309.
22. Hodes, M.; Zhang, R.; Lam, L. S.; Wilcoxon, R.; Lower, N., On the potential of galinstan-based minichannel and minigap cooling. *IEEE Transactions on Components, Packaging and Manufacturing Technology* **2013,** *4* (1), 46-56.
23. Cheng, S.; Rydberg, A.; Hjort, K.; Wu, Z., Liquid metal stretchable unbalanced loop antenna. *Applied Physics Letters* **2009,** *94* (14), 144103.
24. Bo, G.; Ren, L.; Xu, X.; Du, Y.; Dou, S., Recent progress on liquid metals and their applications. *Advances in Physics: X* **2018,** *3* (1), 1446359.
25. Dickey, M. D.; Chiechi, R. C.; Larsen, R. J.; Weiss, E. A.; Weitz, D. A.; Whitesides, G. M., Eutectic gallium-indium (EGaIn): a liquid metal alloy for the formation of stable structures in microchannels at room temperature. *Advanced functional materials* **2008,** *18* (7), 1097-1104.
26. Pan, C.; Markvicka, E. J.; Malakooti, M. H.; Yan, J.; Hu, L.; Matyjaszewski, K.; Majidi, C., A liquid-metal–Elastomer nanocomposite for stretchable dielectric materials. *Advanced Materials* **2019,** *31* (23), 1900663.
27. Bartlett, M. D.; Fassler, A.; Kazem, N.; Markvicka, E. J.; Mandal, P.; Majidi, C., Stretchable, high-k dielectric elastomers through liquid-metal inclusions. *Advanced Materials* **2016,** *28* (19), 3726-3731.
28. Wang, J.; Cai, G.; Li, S.; Gao, D.; Xiong, J.; Lee, P. S., Printable superelastic conductors with extreme stretchability and robust cycling endurance enabled by liquid-metal particles. *Advanced Materials* **2018,** *30* (16), 1706157.
29. Hayashi, Y., Production of natural rubber from Para rubber tree. *Plant Biotechnology* **2009,** *26* (1), 67-70.

30. Rahimi, A.; Mashak, A., Review on rubbers in medicine: natural, silicone and polyurethane rubbers. *Plastics, rubber and composites* **2013,** *42* (6), 223-230.
31. Boley, J. W.; White, E. L.; Kramer, R. K., Mechanically sintered gallium–indium nanoparticles. *Advanced Materials* **2015,** *27* (14), 2355-2360.
32. Thelen, J.; Dickey, M. D.; Ward, T., A study of the production and reversible stability of EGaIn liquid metal microspheres using flow focusing. *Lab on a Chip* **2012,** *12* (20), 3961-3967.
33. Tang, S. Y.; Ayan, B.; Nama, N.; Bian, Y.; Lata, J. P.; Guo, X.; Huang, T. J., On-Chip Production of Size-Controllable Liquid Metal Microdroplets Using Acoustic Waves. *Small* **2016,** *12* (28), 3861-3869.
34. Rane, A. V.; Kanny, K.; Abitha, V. K.; Patil, S. S.; Thomas, S., Clay–polymer composites: design of clay polymer nanocomposite by mixing. In *Clay-Polymer Nanocomposites*, Elsevier: **2017**, pp 113-144.
35. Thomas, P.; Midgley, P., An introduction to energy-filtered transmission electron microscopy. *Topics in catalysis* **2002,** *21* (4), 109-138.
36. Standard, I., Plastics-Determination of tensile properties Part 2: Test conditions for moulding and extrusion plastics. *Reference ISO* **1993**, 527-2.
37. Vaikuntam, S. R.; Bhagavatheswaran, E. S.; Xiang, F.; Wießner, S.; Heinrich, G.; Das, A.; Stöckelhuber, K. W., Friction, abrasion and crack growth behavior of in-situ and ex-situ silica filled rubber composites. *Materials* **2020,** *13* (2), 270.
38. Style, R. W.; Boltyanskiy, R.; Allen, B.; Jensen, K. E.; Foote, H. P.; Wettlaufer, J. S.; Dufresne, E. R., Stiffening solids with liquid inclusions. *Nature Physics* **2015,** *11* (1), 82-87.
39. Eshelby, J. D., The determination of the elastic field of an ellipsoidal inclusion, and related problems. *Proceedings of the royal society of London. Series A. Mathematical and physical sciences* **1957,** *241* (1226), 376-396.
40. Srivastava, S. K.; Mishra, Y. K., Nanocarbon reinforced rubber nanocomposites: detailed insights about mechanical, dynamical mechanical properties, payne, and mullin effects. *Nanomaterials* **2018,** *8* (11), 945.
41. Shtarkman, B.; Razinskaya, I., Plasticization mechanism and structure of polymers. *Acta polymerica* **1983,** *34* (8), 514-520.
42. Paris, P.; Erdogan, F., A critical analysis of crack propagation laws. **1963**.
43. Kazem, N.; Bartlett, M. D.; Majidi, C., Extreme toughening of soft materials with liquid metal. *Advanced Materials* **2018,** *30* (22), 1706594.
44. Clemens, J.; Mawer, C., Granitic magma transport by fracture propagation. *Tectonophysics* **1992,** *204* (3-4), 339-360.
45. Persson, B.; Albohr, O.; Heinrich, G.; Ueba, H., Crack propagation in rubber-like materials. *Journal of Physics: Condensed Matter* **2005,** *17* (44), R1071.
46. González, N.; del Àngels Custal, M.; Lalaouna, S.; Riba, J.-R.; Armelin, E., Improvement of dielectric properties of natural rubber by adding perovskite nanoparticles. *European Polymer Journal* **2016,** *75*, 210-222.
47. Psarras, G., Fundamentals of dielectric theories. In *Dielectric Polymer Materials for High-Density Energy Storage*, Elsevier: **2018**, pp 11-57.
48. Nan, C.-W.; Birringer, R.; Clarke, D. R.; Gleiter, H., Effective thermal conductivity of particulate composites with interfacial thermal resistance. *Journal of Applied Physics* **1997,** *81* (10), 6692-6699.
49. Roland, C., Electrical and dielectric properties of rubber. *Rubber Chemistry and Technology* **2016,** *89* (1), 32-53.
50. Salaeh, S.; Muensit, N.; Bomlai, P.; Nakason, C., Ceramic/natural rubber composites: influence types of rubber and ceramic materials on curing, mechanical, morphological, and dielectric properties. *Journal of materials science* **2011,** *46* (6), 1723-1731.
51. Bartlett, M. D.; Kazem, N.; Powell-Palm, M. J.; Huang, X.; Sun, W.; Malen, J. A.; Majidi, C., High thermal conductivity in soft elastomers with elongated liquid metal inclusions. *Proceedings of the National Academy of Sciences* **2017,** *114* (9), 2143-2148.

52. Plawsky, J. L., *Transport phenomena fundamentals*. CRC press: **2020**.
53. Zeller, R.; Pohl, R., Thermal conductivity and specific heat of noncrystalline solids. *Physical Review B* **1971,** *4* (6), 2029.
54. Kumar, V. B.; Porat, Z. e.; Gedanken, A., DSC measurements of the thermal properties of gallium particles in the micron and sub-micron sizes, obtained by sonication of molten gallium. *Journal of Thermal Analysis and Calorimetry* **2015,** *119* (3), 1587-1592.
55. Tang, S.-Y.; Mitchell, D. R.; Zhao, Q.; Yuan, D.; Yun, G.; Zhang, Y.; Qiao, R.; Lin, Y.; Dickey, M. D.; Li, W., Phase separation in liquid metal nanoparticles. *Matter* **2019,** *1* (1), 192-204.

Table of content (TOC)